Methane chemistry in a nutshell – The new submodels CH4 (v1.0) and TRSYNC (v1.0) in MESSy (v2.54.0)

Franziska Winterstein[1] and Patrick Jöckel[1]

[1]Deutsches Zentrum für Luft- und Raumfahrt (DLR), Institut für Physik der Atmosphäre, Oberpfaffenhofen, Germany

Correspondence: Franziska Winterstein (franziska.winterstein@dlr.de)

Abstract. Climate projections including chemical feedbacks rely on state-of-the-art chemistry-climate models (CCMs). Of particular importance is the role of methane (CH_4) for the budget of stratospheric water vapor (SWV), which has an important climate impact. However, simulations with CCMs are, due to the large number of involved chemical species, computationally demanding, which limits the simulation of sensitivity studies.

To allow for sensitivity studies and ensemble simulations with a reduced demand for computational resources, we introduce a simplified approach to simulate the core of methane chemistry in form of the new Modular Earth Submodel System (MESSy) submodel CH4. It involves an atmospheric chemistry mechanism reduced to the sink reactions of CH_4 with predefined fields of the hydroxyl radical (OH), excited oxygen ($O(^1D)$), and chlorine (Cl), as well as photolysis and the reaction products limited to water vapour (H_2O). This chemical production of H_2O is optionally feed back onto the specific humidity (q) of the connected General Circulation Model (GCM), to account for the impact onto SWV and its effect on radiation and stratospheric dynamics.

The submodel CH4 is further capable of simulating the four most prevalent CH_4 isotopologues for carbon and hydrogen (CH_4 and CH_3D as well as $^{12}CH_4$ and $^{13}CH_4$), respectively. Furthermore, the production of deuterated water vapour (HDO) is, similar to the production of H_2O in the CH_4 oxidation, optionally passed back to the isotopological hydrological cycle simulated by the submodel H2OISO, using the newly developed auxiliary submodel TRSYNC. Moreover, the simulation of a user defined number of diagnostic CH_4 age and emission classes is possible, which output can be used for offline inverse optimization techniques.

The presented approach combines the most important chemical hydrological feedback including the isotopic signatures with the advantages concerning the computational simplicity of a GCM, in comparison to a full featured CCM.

1 Introduction

It is beyond question that methane (CH_4) is a strong greenhouse gas (GHG), with an estimated global warming potential (GWP) of 34 times that of carbon dioxide (CO_2) on a 100 year horizon (IPCC, 2013). Therefore, most General Circulation Models (GCMs) include the effect of the radiative forcing of CH_4. However, the effect of CH_4 is underrepresented by only

using its direct radiative impact and not accounting for the water vapour (H_2O) produced by the oxidation of CH_4 due to a set-up without chemistry. Especially in the stratosphere this additional H_2O (stratospheric water vapor (SWV)) influences among others the radiative forcing, stratospheric temperature and the ozone (O_3) chemistry (Stenke and Grewe, 2005; Tian et al., 2009; Solomon et al., 2010; Revell et al., 2012; Winterstein et al., 2019). The inclusion of production of H_2O by CH_4 requires a chemical mechanism as provided by chemistry-climate models (CCMs). Current state-of-the-art CCMs include a vast amount of chemical species and reactions. By extending the chemical mechanisms, one intends to achieve an increase in accuracy of the atmospheric chemistry representation. At the same time, however, the computational demands increase. Although, available computational power increases at a certain rate, too, the availability and capacity of high performance computers is a limiting factor for sensitivity studies in climate projection simulations with CCMs.

It is hence advisable to recognize both main effects of CH_4, namely its radiative forcing and its impact on SWV, but keeping computational demands low at the same time. Therefore, our approach to simulate CH_4 includes both effects and is able to use predefined reaction partners of CH_4, which reduces computational cost to a minimum.

An early version of the simplified CH_4 chemistry submodel (CH4) has been described by Eichinger et al. (2015a). The present version has been updated and extended by the additional features for simulating age and emission classes and isotopologues.

Sections 1.1 and 1.2 introduce the sources and sinks of CH_4, and CH_4 isotopologues and their fractionation effects, respectively. In Sect. 2 we briefly present the Modular Earth Submodel System and describe the concept of the CH4 submodel in Sect. 3. Two additional options of the CH4 submodel are explained in the subsequent Sects. 3.1 and 3.2. The coupling to the hydrological cycle with the submodel TRSYNC is introduced in Sect. 4. We show three example applications using the newly presented submodels in Sect. 5 and end with a short summary. Parts of the manuscript are based on the PhD thesis of the first author (Frank, 2018).

1.1 Sources and sinks of CH_4

Methane is a GHG emitted by both natural, and anthropogenic sources at the Earth's surface. There are basically no known chemical sources of CH_4 in the free atmosphere.

In CCMs usually predefined lower boundary conditions instead of emission fluxes are used to describe atmospheric CH_4. This approach is mainly employed due to two major problems: (1) The lifetime of CH_4 is in the order of magnitude of 10 years, but its exact value is still unknown and subject to uncertainties. However, CH_4 is an important precursor of the Ox/HOx chemistry in CCMs. For this reason, in most CCM setups, CH_4 is prescribed at the lower model boundary to achieve a realistic CH_4 burden independent of the simulated lifetime. (2) Despite large ongoing efforts, current emission inventories are still subject to large uncertainties, as top-down and bottom-up inventories differ significantly (e.g. EDGAR or Saunois et al. (2016)). This mismatch indicates the dilemma, that there are a lot of open questions with respect to both, the magnitude of sources, and the sinks of CH_4.

Methane is removed from the atmosphere mainly by three photochemical reactions:

$$CH_4 + OH \overset{k_{CH_4+OH}}{\rightarrow} CH_3 + H_2O \quad \text{(R1)}$$

$$CH_4 + O(^1D) \overset{k_{CH_4+O(^1D)}}{\rightarrow} products \quad \text{(R2)}$$

$$CH_4 + Cl \overset{k_{CH_4+Cl}}{\rightarrow} CH_3 + HCl \quad \text{(R3)}$$

and is also depleted by photolysis:

$$CH_4 + h\nu \overset{j_{CH_4+h\nu}}{\rightarrow} products \quad \text{(R4)}$$

with (R1)–(R3) from (Sander et al., 2011) and (R4) from (Sander et al., 2014).

About 92 % of the atmospheric CH_4 removal happens in the troposphere. The largest part is thereby the reaction with the hydroxyl radical (OH) (>90 % of the tropospheric sink), while the rest is attributed to the reaction with chlorine (Cl) in the Marine Boundary Layer (MBL, Kirschke et al. (2013)). About 8 % of CH_4 is depleted in the stratosphere, by the reactions with OH, excited oxygen ($O(^1D)$), Cl and through photolysis (IPCC, 2013).

Another sink of CH_4 is the so called soil-loss at the Earth's surface. CH_4 is either depleted by CH_4 consuming bacteria (methanotrophs), or it is removed from the air by diffusive transport into the soil, which is mostly influenced by soil water content (King, 1997). Globally, the soil-loss accounts for approximately 4 % of the total CH_4 sink (IPCC, 2013).

1.2 Isotopologues of CH_4

A powerful and common method in the investigation of the CH_4 budget is the study of CH_4 isotopologues. Production and removal of CH_4 cause fractionation effects, which lead to distinct isotopological signals in the atmosphere. These isotopic signatures provide potentially additional insights into the role of specific CH_4 sources and depleting reactions, and are already widely used in the context of CH_4 (Hein et al., 1997; Fletcher et al., 2004; Monteil et al., 2011; Rigby et al., 2012; Nisbet et al., 2016; Schaefer et al., 2016).

Fundamentally, the stable isotopologues of CH_4 form with respect to the most abundant stable isotopes of hydrogen and of carbon. The stable isotopes of hydrogen are ^{1}H and ^{2}H (deuterium, D), and for carbon, carbon-12 (^{12}C) and carbon-13 (^{13}C). This results in the first order stable isotopologues $^{12}CH_4$, $^{13}CH_4$, and CH_3D. The corresponding sink reactions are shown in the supplement section S1. The relative abundances of higher substituted and mixed isotopologues (e.g. CH_2D_2 or $^{13}CH_3D$) are less than 0.0007% (compared to 0.0616% of CH_3D) (Stolper et al., 2014) and hence neglected.

The chemical fractionation is based on the fact that isotopologues of the same molecule have different rate coefficients, i.e. they react with different speed or probability. This difference in rate coefficients is described as the so called Kinetic Isotope Effect (KIE) and becomes apparent during the chemical reaction of a specific molecule X:

$$X_L + E \overset{k_L}{\rightarrow} P \quad \text{(R5)}$$

$$X_H + E \overset{k_H}{\rightarrow} P' \quad \text{(R6)}$$

with X_L being its light (major), and X_H its heavy (minor) isotopologue. E and P/P' denote the reaction partner(s) and product(s), respectively. The value of the KIE is thereby defined as the ratio of the rate coefficients k_L and k_H (Bigeleisen, 2005)

Table 1. Temperature dependent KIEs of the sink reactions of CH_4 described as $\mathrm{KIE} = \mathrm{A} \cdot \exp(\mathrm{B}/T)$. The KIEs are valid in the given temperature range (T in [K]).

reaction	A	B	T	reference
$\mathrm{KIE}^{\mathrm{OH}}_{^{13}CH_4}$	1.0039	0.0	200–300	(Saueressig et al., 2001)
$\mathrm{KIE}^{\mathrm{O(^1D)}}_{^{13}CH_4}$	1.013	0.0	223–295	(Saueressig et al., 2001)
$\mathrm{KIE}^{\mathrm{Cl}}_{^{13}CH_4}$	1.043	6.455	223–297	(Saueressig et al., 1995; Crowley et al., 1999)
$\mathrm{KIE}^{\mathrm{OH}}_{CH_3D}$	1.097	49.0	249–422	(Saueressig et al., 2001)
$\mathrm{KIE}^{\mathrm{O(^1D)}}_{CH_3D}$	1.060	0.0	224–295	(Saueressig et al., 2001)
$\mathrm{KIE}^{\mathrm{Cl}}_{CH_3D}$	1.278	51.31	223–295	(Saueressig et al., 1996)

and its inverse is called the fractionation factor α:

$$\mathrm{KIE} := \frac{k_L}{k_H} = \frac{1}{\alpha} \,. \tag{1}$$

The KIEs of the sink reactions of CH_4 have been, among others, determined by Saueressig et al. (1995, 1996, 2001) and Crowley et al. (1999) in laboratory measurements (see Table 1). Since the KIEs of CH_4 isotopologues are partly temperature dependent, the KIEs are described by two parameters A and B and are calculated as

$$\mathrm{KIE} = \mathrm{A} \cdot \exp(\mathrm{B}/T), \tag{2}$$

with T being the temperature in [K].

The largest KIE and therefore strongest fractionation effect is found for the reaction with Cl, which especially influences the isotopic composition of CH_4 in the middle and upper stratosphere (Saueressig et al., 1996; Bergamaschi et al., 1996). Conversely, the reaction with O(^{1}D) shows the lowest KIE, which furthermore does not show any temperature dependence. The KIE of the reaction with OH is temperature dependent with respect to deuterated methane (CH_3D) but not with respect to methane containing ^{13}C ($^{13}CH_4$) (Saueressig et al., 2001). Nair et al. (2005) estimated the rate coefficients of the photodissociation of CH_4 and its major isotopologues for planet Mars, which results in a calculated KIE$= 1.005$ for CH_3D and a negligible isotopic fractionation for the ^{13}C isotopologue (Nixon et al., 2012). There is, especially for deuterium, a non-negligible fractionation during the soil-loss for CH_4 (Snover and Quay, 2000; Maxfield et al., 2008). An average value for the overall soil-loss is estimated as $\mathrm{KIE}^{\mathrm{soil}}_{CH_3D} = 1.0825$ and $\mathrm{KIE}^{\mathrm{soil}}_{^{13}CH_4} = 1.0196$ (Snover and Quay, 2000; Holmgren, 2006; Maxfield et al., 2008).

2 The Modular Earth Submodel System (MESSy)

The framework of the Modular Earth Submodel System (MESSy, used in the second version MESSy2, Jöckel et al. (2010)) is based on the idea to modularize a climate model in a way, that single components can be switched on and off independently, depending on the desired set-up, meeting the demands of current Earth System Modeling in terms of flexibility and

computational performance. The modularization enables the user to pick suitable submodels or expand the model easily with new ones. Presented here are the submodel CH4 and the auxiliary submodel TRacer SYNChronization (TRSYNC), which are implemented based on this framework.

For the application examples of the new submodels, MESSy is used together with the 5th generation European Centre Hamburg general circulation model (ECHAM5, Roeckner et al. (2006)). The ECHAM/MESSy Atmospheric Chemistry (EMAC) model is a numerical chemistry and climate simulation system that includes sub-models describing tropospheric and middle atmosphere processes and their interaction with oceans, land and human influences (Jöckel et al., 2010). EMAC (ECHAM5 version 5.3.02, MESSy version 2.54, Jöckel et al. (2010, 2016)) is applied in the given examples in the T42L90MA-resolution, i.e. with a spherical truncation of T42, which corresponds to a quadratic Gaussian grid of approx. 2.8 by 2.8 degrees in latitude and longitude, and includes 90 vertical hybrid pressure levels from the Earth surface up to 0.01 hPa. MESSy allows the configuration of EMAC in several operational modes. The two basic ones are the GCM set-up without chemistry and the CCM set-up with fully interactive chemistry, using, among other components, the Module Efficiently Calculating the Chemistry of the Atmosphere (MECCA, Sander et al. (2005)) and the SCAVenging (SCAV, Tost et al. (2006)) submodel to represent the chemical kinetics of EMAC in gas phase and in aqueous phase, respectively. They define the underlying chemical reaction mechanisms in troposphere, stratosphere, and lower mesosphere. MECCA and SCAV provide comprehensive mechanisms, combining state-of-the-art reactions and rate coefficients. The kinetic chemistry tagging technique (MECCA_TAG, Gromov et al. (2010)) enables the user to tag selected chemical elements, without modifying the underlying standard chemical mechanism of MECCA. It can be applied for simulating isotopologues of trace gases with respect to selected isotopes. In order to do so, rare and abundant isotopologues of the species of interest (e.g., those containing atomic hydrogen (H)) are created in an extended set of reactions in the same chemical mechanism.

MESSy and its application in EMAC has been used in multiple studies (see the special issue in Atmospheric Chemistry and Physics https://www.atmos-chem-phys.net/special_issue22.html) and includes several submodels from contributing institutions. Further information on EMAC, MESSy and its submodels can be found in Jöckel et al. (2010, 2016), on the web-site https://www.messy-interface.org/, or accompanying papers documenting the specific submodels.

3 The submodel CH4

The MESSy submodel CH4 aims to close the gap between the operational modes of EMAC as a GCM without chemistry and as a CCM with the comprehensive chemical mechanisms of MECCA and SCAV. The basic concept of the submodel is to limit the chemical mechanism to the loss-processes of methane and use predefined fields of the reaction partners OH, O(^{1}D) and Cl to reduce the computational demands.

The sink reactions (R1)–(R4) in the CH4 submodel are parameterized as follows:

$$\frac{d[CH_4]}{dt} = (-k_{CH_4+OH} \cdot c_{\text{air}} \cdot [OH] - k_{CH_4+O(^1D)} \cdot c_{\text{air}} \cdot [O(^1D)] - k_{CH_4+Cl} \cdot c_{\text{air}} \cdot [Cl] - j_{CH_4+h\nu}) \cdot [CH_4], \quad (3)$$

where [X] denotes the mixing ratio of species X in [mol mol^{-1}], c_{air} the concentration of air in [cm^{-3}], k_{R} the reaction rate coefficient of reaction R in [cm^3 s^{-1}] and $j_{CH_4+h\nu}$ the photolysis rate of CH_4 in [s^{-1}].

The prescribed fields are taken either from existing simulation results with detailed chemistry, or from other data sources (e.g. reanalyses or projections). If CH4 is included in an EMAC CCM simulation (which is possible in the MESSy framework), the CH4 submodel can also be coupled to the reactant fields, which are on-line calculated during the same simulation by the chemical mechanism (i.e. MECCA). Although this does not save computational requirements, such a simulation configuration can be used, for example, if output of one of the additional options of the CH4 submodel (age and emission classes or isotopologues) are desired. In that case a second CH_4 tracer is treated and oxidized by the reactants provided by the kinetic solver of the comprehensive chemical mechanism. The same applies for the photolysis rate of CH_4, which can be prescribed from offline provided gridded data or on-line calculated by the submodel JVAL (Sander et al., 2014). In either case, the CH4 submodel does not alter the reactant educts. Hence there is no feedback onto the CH_4 sink by the submodel. In case of coupling to MECCA via the educts the coupling is one-way only.

Figure 1 visualizes the conceptual differences between the MESSy submodel CH4 (left) and a CCM simulation with MECCA (right). MECCA simulates the entire chemical mechanism and therefore also includes the feedback onto the reaction partners (depicted in yellow) of CH_4. Additionally, there is also a secondary feedback by the products from the CH_4 sink reactions (e.g., H_2O, HO_2, depicted in blue), as the subsequent chemical processes are influenced by the products from the CH_4 oxidation. Conversely, the CH4 submodel uses the prescribed fields of the reactant species to calculate the CH_4 loss. This loss is included in the master tracer of the CH4 submodel (the present CH_4 is reduced), but does not feedback onto the sink fields or any other chemical species. The only exception is H_2O, in the case when the hydrological feedback of CH_4 oxidation is switched on. GCMs include CH_4 foremost for its radiative impact as a greenhouse gas, but also for its influence on stratospheric water vapor (SWV, e.g. Monge-Sanz et al. (2013); ECMWF (2007); Austin et al. (2007); Boville et al. (2001); Mote (1995)). The CH4 submodel is therefore equipped with an optional feedback onto H_2O, to account for part of the secondary climate feedback of CH_4. It is thereby assumed that two molecules of H_2O are produced per oxidized CH_4 molecule (le Texier et al., 1988), which is, however, only a rough approximation as analyzed by Frank et al. (2018). The approximation of two molecules H_2O per oxidized CH_4 molecule overestimates the H_2O production in the lower stratosphere and underestimates the production in the upper stratosphere. It also does not account for the chemical loss of H_2O in the mesosphere.

Note that soil loss is not explicitly included in the CH4 submodel, since the concept of dry deposition is already part of the EMAC submodel DDEP (Kerkweg et al., 2006a). An example how to use DDEP to simulate the soil loss of CH_4 is included in the supplement of this paper.

The submodel CH4, with its four sink reactions of CH_4, is considerably computationally cheaper, compared to a fully interactive chemistry simulation using MECCA, which represents (depending on the chosen set-up) several hundred reactions (e.g., more than 300 in the base simulations of Earth System Chemistry integrated Modelling (ESCiMo) project (Jöckel et al., 2016)). For example, a reference set-up with MECCA requires about 250 node-h[1] per simulated year, while a set-up with the CH4 submodel without MECCA requires only 30 node-h per year (these numbers are calculated for simulations conducted on the high performance computer (HPC) Mistral at the *Deutsches Klimarechenzentrum* (DKRZ)).

[1] node-h: required wall-clock hours times applied high performance computer (HPC) nodes.

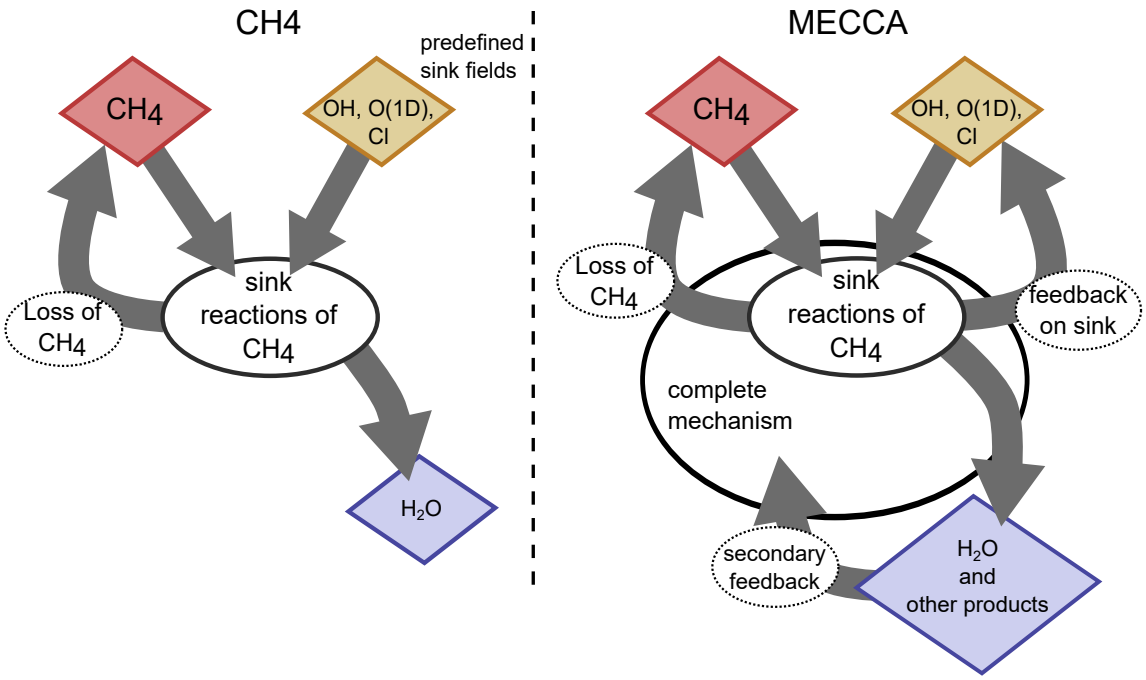

Figure 1. Sketch visualizing the concepts of parameterizing CH_4 sink reactions in the MESSy submodels CH4 (left) and MECCA (right). The red species is the core species CH_4. The chemical mechanism in CH4 is reduced to the sink reactions of CH_4 and optionally includes the feedback to H_2O (blue) only. In MECCA a complete chemical mechanism is included, which feeds back among others on H_2O and other products of the CH_4 sink reactions including the reaction partners (educts) of CH_4. The reaction partners (yellow) in the CH4 submodel are prescribed and not changed by the CH4 submodel.

The presented framework of the reduced CH_4 chemistry is applicable, since CH_4 is only reduced and not produced in the free atmosphere. Therefore the discretization of the four reactions, where CH_4 is involved, is sufficient to represent the chemical loss of CH_4. Nevertheless, in order to achieve meaningful simulation results with the CH4 submodel some prerequisites have to be met. Since the educts (OH, Cl and $O(^1D)$) are prescribed, there is no feedback on them. Thus, very large variations in CH_4 mixing ratio, which would in reality influence the CH_4 sink (Winterstein et al., 2019), are not representable by the CH4 submodel.

Furthermore, the setup with the CH4 submodel also lacks any feedback on O_3. In the atmosphere, the O_3 chemistry is influenced by changes in OH (reduced by CH_4), H_2O (produced by CH_4) and temperature (influenced by the radiatively active CH_4). The CH4 submodel alters H_2O and with that influences the radiation budget and hence the temperature, however, there is no feedback on O_3 when the setup does not include any other chemical mechanism. In a setup where the CH4 submodel is not used in parallel to MECCA, O_3 time series or climatologies are usually prescribed for the radiation scheme.

First simulations using the CH4 submodel are presented in studies by Eichinger et al. (2015a, b), it was included in the simulations of the ESCiMo project (Jöckel et al., 2016) and it has been used for the CH_4 forecast system presented by Nickl et al. (2019).

3.1 Option I: Age and Emission classes

The CH_4 submodel includes an option for simulating age and emission classes. These classes, which can be specified by the user via a namelist, enable a precise distinction between CH_4 source sectors and/or regions (emission classes), as well as further insight into the CH_4 distribution over time (age classes). The term "emission class" thereby denotes a CH_4-like tracer defined by the CH4 submodel. The assignment of specific emission fluxes (sectors and regions) to the tracers of the emission classes is handled by the submodel OFFEMIS (Kerkweg et al., 2006b). In our present application example these classes are subject to emissions being a combination of an emission sector (like wetlands, biomass burning, anthropogenic etc.) and a region (e.g. continents or countries). One tracer, for example, thus traces anthropogenic CH_4 emitted from Africa, as shown in Sect. 5.1. These additional diagnostic tracers are transported identically to the master CH_4 tracer of the CH4 submodel and also experience the same sink reactions.

The time period represented by one age class can be chosen by the user. How the age and emission classes evolve over time is depicted in Fig. 2. Methane of each emission class is propagated through a specific number of age classes. The emitted CH_4 of a specific emission class is added to the tracer which corresponds to the first age class. After the selected time span it moves to the next "older" age class until it reaches the oldest. The oldest age class represents the background, since CH_4 does not proceed further.

It is further selectable which age evolving method is applied. The CH4 submodel offers three options: (1) CH_4 is passed on in one step after a user-defined time-span, (2) CH_4 is continuously passed on with respect to an user-defined time-span, and (3) CH_4 is passed on monthly with fixed time lag.

We define the state vector for emission class i and age classes 1 to N as:

$$f_i = \begin{pmatrix} f_{i1} \\ f_{i2} \\ \vdots \\ f_{iN} \end{pmatrix} \tag{4}$$

The first two options are implemented according to

$$\Delta f_i = \frac{M \cdot f_i}{\Delta t}, \tag{5}$$

with Δf_i being the tendency of f_i, Δt being the time step length, and M being a matrix defining the ageing step according to the chosen option. For option (1) this matrix looks like

$$M = \begin{pmatrix} -1 & 0 & & \cdots & & 0 \\ 1 & -1 & & & & \\ & 1 & -1 & & & \vdots \\ & & & \ddots & \ddots & \\ 0 & & \cdots & & 1 & 0 \end{pmatrix}. \tag{6}$$

This moves the current values of one age class tracer after a user-defined time-span to the next older one. This option is not consistent with a Leapfrog time stepping using an Asselin-filter and might cause numerical oscillations and negative values. It was implemented solely for testing purposes during development, but it is not recommended for real applications. The ageing step matrix M for option (2) is M'

$$M' = \alpha \cdot M, \tag{7}$$

with $\alpha = \frac{\Delta t}{\tilde{T}}$ and $\tilde{T}$ being the user-defined time-span indicating the binning width of the age class. This option carries out a quasi-continuous update of the age classes, as it moves at every time step a fraction (α) of the current age class to the next.

The third option is implemented for usage by a fixed-lag Kalman filter for inverse optimization. With this option, one age class represents one month and at the end of one month all CH_4 of one age class moves to the next. This option is specifically implemented to be consistent with the Leapfrog time stepping (c.f. option (1)). A preliminary application of the concept of using the age and emission classes for an inverse optimization using the fixed-lag Kalman Filter has been shown by Frank (2018).

In order to reduce numerical errors, the age and emission classes are continuously constrained (i.e., in each model time step) to sum up to the master tracer and are scaled appropriately, if the sum deviates. This procedure is done to avoid the accumulation of such numerical errors, which mainly arise from small non-linearities of the large scale advection scheme. The magnitude therefore depends on the applied advection scheme, but is usually of the order of floating point precision.

3.2 Option II: Isotopologues

Additional to solving the basic CH_4 kinetics, the submodel CH4 further allows for the simulation of CH_4 isotopologues, which are a potent diagnostic measure in the source and sink attribution. The submodel CH4 is able to simulate the abundant and first order rare isotopologues and defines these as tracers additional to the master tracer. Higher substituted isotopologues are neglected. The user can choose whether isotopologues are simulated with respect to carbon (methane containing ^{12}C ($^{12}CH_4$) and $^{13}CH_4$), or hydrogen (CH_4 (containing ^{1}H isotopes only) and CH_3D), or both. The abundant (with ^{12}C or ^{1}H isotopes only) and rare (with ^{13}C or D) isotopologues are thereby simulated in parallel. During the simulation it is taken care that each isotopologue family sums up to the master tracer CH_4 tracer of the CH4 submodel (`CH4_fx`). The isotopic signatures of CH_4 emission sources are included by splitting the emission fluxes into an abundant and a rare fraction. This is handled via the OFFEMIS namelist (Kerkweg et al. (2006b), see example namelists in the supplement).

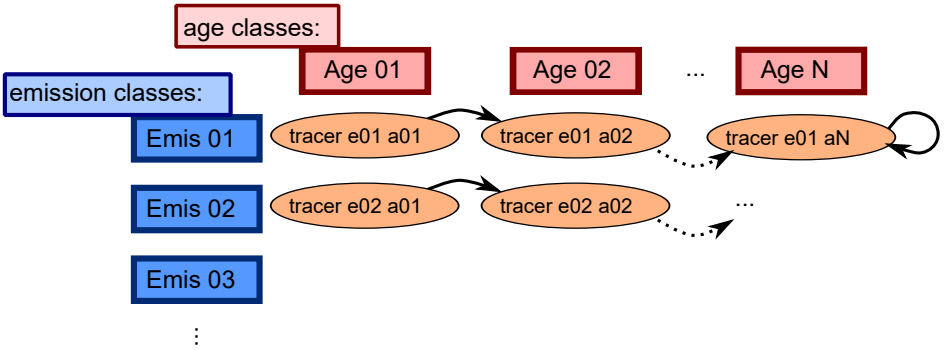

Figure 2. Sketch showing the advancing of the age classes in the CH4 submodel. Each tracer represents one specific emission and age class. After the defined length of time, the age classes proceed to the next "older" age class. The last class represents the background CH_4, where the CH_4 is only subject to transport and the chemically defined sink reactions, but not propagated to an older age class, which is indicated by the circled arrow.

The rate coefficients of the CH_4 isotopologues with their reaction partners are adjusted with respect to the KIE factors, e.g.:

$$\text{KIE} = k_{\text{CH}_4+\text{OH}} / k_{\text{CH}_3\text{D}+\text{OH}} \,, \tag{8}$$

and similar for reactions with O(^{1}D), Cl, and photolysis. The applied reaction partners are thereby the same as those used for the master tracer.

The oxidation of CH_3D produces to a certain extent deuterated water vapour (HDO). If the feedback of CH_4 oxidation onto the hydrological cycle and the simulation of D containing isotopologues is switched on in the CH4 submodel, an additional tracer for HDO is created by the submodel and filled by the produced HDO from CH_3D oxidation. There are two options available: (1) one oxidized CH_3D produces one HDO molecule, or (2) the tendency of the HDO tracer is calculated by Eq. (9) (Eichinger et al., 2015a):

$$\frac{\partial(HDO)}{\partial t} = \frac{-\frac{\partial(CH_3D)}{\partial t} + 6.32 \times 10^{-5} \cdot \frac{\partial(CH_4)}{\partial t}}{\frac{M_{air}}{M_{HDO}} \left(\frac{1}{1-HDO}\right)^2} \,, \tag{9}$$

with M_{air} and M_{HDO} being the molar masses of air (28.987 g mol^{-1}) and HDO (19.02 g mol^{-1}), respectively. This empirical equation accounts for the D, which stays in deuterated molecular hydrogen (HD), as it builds up to an equilibrium with HDO via the HOx-cycle.

4 Coupling to the hydrological cycle with the new submodel TRSYNC

In EMAC three different submodels are included dealing with isotopologues of H_2O in the vapor phase: (1) the CH4 submodel presented here, (2) MECCA_TAG, and (3) H_2O ISOtopologues (H2OISO, Eichinger et al. (2015a)). CH4 and MECCA_TAG include the chemical fractionations, while H2OISO is responsible for the physical fractionations in the hydrological cycle of

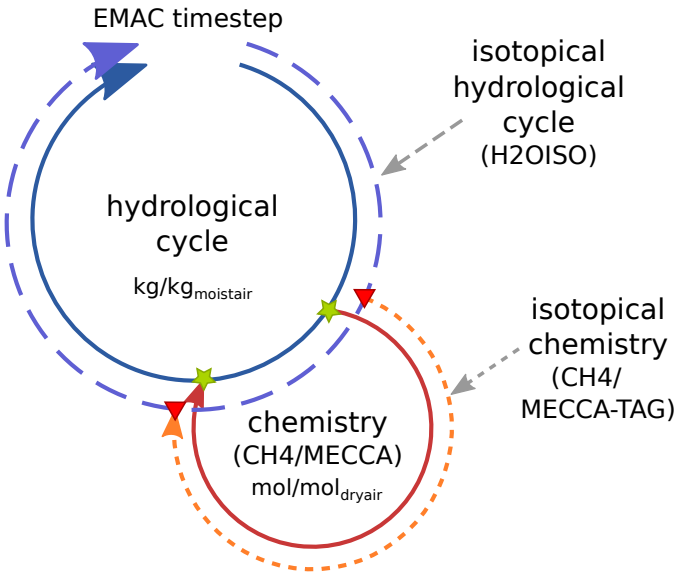

Figure 3. Sketch showing the coupling of the hydrological cycle and the chemistry (either CH4 or MECCA) with respect to H_2O isotopologues in one time step of EMAC. Green stars indicate the points of the hydrological cycle, where (1) the current value of the water vapor master tracer is taken, and (2) the chemical tendencies are added onto the water vapor master tracer. Red triangles indicate the synchronization points of the corresponding isotopical tracers by the TRSYNC submodel. Synchronization of the isotopological cycles accounts also for the appropriate unit conversion and adds the tendency of chemical processes to the fractionation in the physical hydrological cycle.

the underlying GCM. All three create independent tracers of H_2O isotopologues, which need to be synchronized to be able to combine physical and chemical fractionation effects of H_2O and its isotopologues. The chemical fractionation is thereby considered either from MECCA_TAG or from CH4, although both submodels can be concurrently included in a simulation and compute the isotopic fractionation independently.

In principal, if EMAC is applied in GCM mode, only the master hydrological cycle is present (see Fig. 3, inner solid blue cycle). Adding MECCA or CH4 to the set-up expands the model into a CCM, or a simple "CH_4-only" CCM, respectively (red solid circle). The chemistry submodels use water vapor as a chemical tracer (first green star) and calculate the contribution from CH_4 oxidation (second green star). This chemical feedback onto water vapor was already implemented as an option in previous EMAC versions. By including the isotopological submodels into the set-up, H2OISO duplicates the hydrological cycle for the water isotopologues and CH4 or MECCA_TAG create the chemical tracers of the water isotopologues (outer dashed circles). This results in several physical and chemical H_2O isotopologue tracers. While the master chemical process adds its feedback directly to the specific humidity of the hydrological cycle (there is no need for a chemical water tracer), the synchronization of the physical isotopological tracers in the isotopic hydrological cycle (H2OISO) and the chemical isotopological tracers (CH4 or MECCA_TAG) is done via the new auxiliary submodel TRSYNC. In brief, TRSYNC guarantees that the physical H_2O tracers (incl. their isotopologues) receive also the correct tendencies of the corresponding chemical tracers. Since isotopological water

vapor tracers of MECCA_TAG and the HDO tracer created by CH4 are transported in EMAC in the same way as every other tracer, they are subject to some of the physical processes, but not to all hydrological fractionation effects. Thus, at the first synchronization point the chemical tracer is synchronized to represent the current value of the physical tracer. In the following, chemical tendencies including fractionation effects are calculated and are added via the second synchronization point to the physical tracer. By doing so, chemical and physical fractionation processes are strictly separated and the tendencies of the chemical tracers represent the chemical tendencies in addition to the previous physical fractionations in the current time step.

Water vapor in the physical hydrological cycle (regarding ECHAM5 and H2OISO) are defined in units of kg of the tracer per kg of moist air (kg $kg^{-1}_{\text{moist air}}$), while the chemical tracers are defined in mol mol^{-1}_{dryair}. This also holds for the corresponding isotopologue tracers. Parameterizations of physical processes in ECHAM5 are by design formulated with specific humidity (per moist air). Conversely, chemical reactions are necessarily calculated with species concentrations. This requires the individual chemical and physical isotopologue tracers, which have, for the sake of correct process formulations, distinct units, and motivated the development of the auxiliary submodel TRSYNC in order to be able to synchronize these tracers accordingly and in a common way for CH4 and MECCA_TAG, respectively.

In addition to that, the application of MECCA_TAG creates the basis to investigate various other isotopes in the interactive chemical mechanism. While CH4 feedbacks on H_2O with respect to hydrogen isotopes only, MECCA_TAG can also be used to simulate oxygen isotopes (^{16}O, ^{17}O and ^{18}O) in the chemical mechanism. It is therefore also possible to couple MECCA_TAG with oxygen isotopes to the corresponding oxygen related isotopologue tracers in H2OISO. Last but not least, for MECCA_TAG tracer names are not standardized. Therefore, the namelist of the submodel TRSYNC can be adjusted according to the actual tracer names used in MECCA_TAG.

5 Example applications

The following examples are simulations carried out with EMAC in a GCM-like mode including the newly presented CH4 and TRSYNC submodels. Other involved MESSy submodels are OFFEMIS (Kerkweg et al., 2006b) and DDEP (Kerkweg et al., 2006a). OFFEMIS manages the emissions of CH_4 from prescribed sources. It reads predefined fields with emission data and adds these fluxes to the chemical tracers. DDEP simulates the dry deposition for gases and aerosols and is used in the present context to simulate the soil-loss of CH_4, which is not done in the CH4 submodel itself.

Monthly mean sink fields are used in the simulation set-up in the examples below. Higher frequencies are technically possible, this would, however, increase the computational demands due to the larger amount of data read from disk. Monthly mean fields smooth the diurnal cycle, which is especially strong in OH. However, in order to investigate long-term global trends of CH_4, which has a tropospheric lifetime of 8–10 years, variations on time scales of less than one month are negligible and monthly mean fields are assumed to suffice for such applications. Furthermore in the examples, photolysis rates are calculated by the submodel JVAL in the presented examples, but predefined data can be used as well.

The H2OISO submodel (Eichinger, 2014; Eichinger et al., 2015a) simulates the stable water isotopologues with respect to H and D, as well as ^{16}O, ^{17}O and ^{18}O. Overall, it represents a second hydrological cycle, which includes water isotopologues

in their three phases: gas, liquid and ice. H2OISO accounts for fractionation processes during phase transitions in large scale and convective clouds, during vertical diffusion, and during evaporation from the ocean (evaporation from soil, biosphere and snow are not considered to have a significant fractionation).

We simulated the years 1989 to 2012 and applied a specified dynamics set-up to represent the reanalyzed meteorology of this time. Specified dynamics means here that the prognostic variables divergence, vorticity, temperature and (logarithm of) surface pressure are nudged by Newtonian relaxation towards ECMWF ERA-Interim reanalysis data (Dee et al., 2011).

5.1 Application of the CH4 submodel for inverse optimization of CH_4 emission inventories

Current estimates of CH_4 emission inventories still include large uncertainties. In order to reduce these, new estimates of inventories must be able to represent temporal and spatial resolutions in greater detail (e.g., seasonal cycle, distinct regions). One statistical method to estimate CH_4 emission strengths is the fixed-lag Kalman Filter, which performs an inverse optimization of the emission inventory by comparing simulated and observed mixing ratios of a trace gas (see e.g., Bruhwiler et al. (2005)). This "off-line" inversion algorithm requires data from a forward simulation including temporal and spatial information of the simulated CH_4 tracer.

In order to provide the necessary data, the CH4 submodel with the option of age and emission classes is applied. The combination of chosen regions and emission sectors in this example results in 48 emission classes altogether. These 48 emission classes are simulated with 5 age classes for ages up to 1, 2, 3, 4, and $\geq$5 months since emission release. Figure 4 shows exemplarily the evolution of one emission class (i.e., anthropogenic emissions in Africa) from age class to age class. Panel (a) shows the emissions of the year 2000 in g(CH_4) m^{-2} per year (y^{-1}). The other panels (b)–(f) show the age classes in ascending order and display the distribution of the CH_4 mixing ratio onto the 5 age classes in January 2000 (the simulation has started in 1989). In the fourth age class the CH_4 from anthropogenic African sources is almost evenly distributed mostly in the Northern Hemisphere (NH). Eventually, the fifth (i.e. the last age class) shows the accumulated background of all CH_4 from anthropogenic African sources. Applied is an a priori emission inventory.

Overall, the temporal evolution of the age classes in Fig. 4 confirms that the 5 age classes in this set-up sufficiently track the spread of CH_4 towards a fairly uniform distribution, which is a prerequisite for a successful application of the inverse optimization method.

5.2 Simulating CH_4 isotopologues

We further present a simulation using the CH4 submodel, which includes all four CH_4 isotopologues. For this simulation, we applied a global a posteriori emission inventory provided by Dominik Brunner (pers. communication) and a set of isotopic emission signatures prepared from data from literature (see Table S1 in the supplement). Figure 5 shows zonal mean climatologies (2000–2009) of CH_4 in [nmol mol^{-1}] and the corresponding isotopic signature in [‰]. The isotopologues are displayed in the δ-notation with respect to the reference isotope ratios Vienna-PeeDee Belemnite (VPDB) for $^{13}CH_4$, and Vienna Standard Mean Ocean Water (VSMOW) for CH_3D, respectively. In the troposphere the NH is isotopically depleted compared to the Southern Hemisphere (SH). Most isotopically light emissions, as for example wetlands and rice, are located in the NH, while

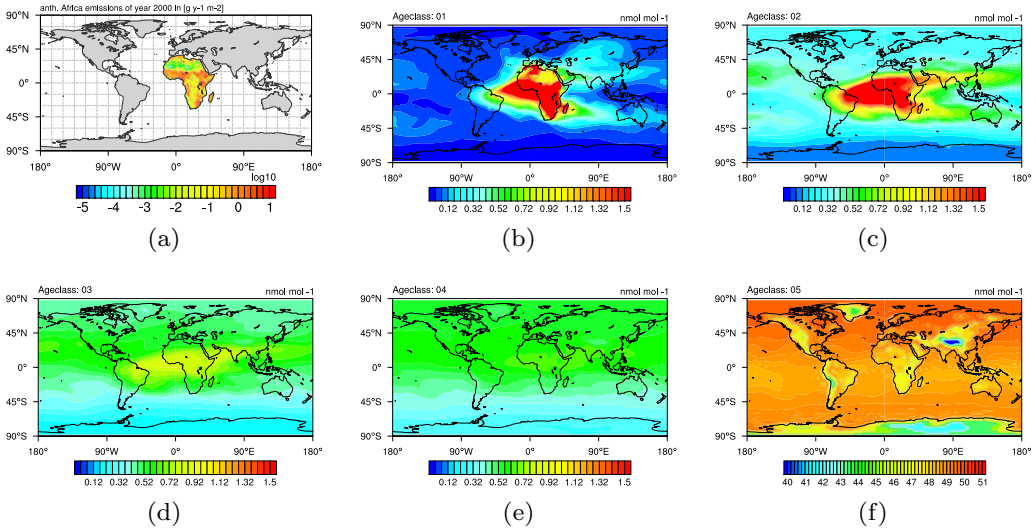

Figure 4. Panel (a): anthropogenic emissions in Africa (taken from EDGARv4.2 2010 fast track database (Olivier and Janssens-Maenhout, 2012)). Panels (b)–(f): Methane as pressure weighted column up to 200 hPa of anthropogenic origin from Africa, distributed into 5 age classes, i.e. up to 1, 2, 3, and 4, and $\geq$5 months after emission release. Shown are exemplarily all age classes of January 2000 after the simulation has run for 12 years.

isotopical heavy sources like biomass burning are mostly located in the SH. This results in the prevalent tropospheric North-South gradient. In the stratosphere CH_4 becomes isotopically enriched towards higher altitudes. When CH_4 is ascending in the atmosphere it is exposed to oxidation. Due to fractionation processes heavy CH_4 isotopologues are unfavored and therefore accumulate in the remaining CH_4.

Our simulation results compare well to observations. For example isotopic observations from the National Oceanic and Atmospheric Administration/Earth System Research Laboratory (NOAA/ESRL) sampling sites (White et al., 2016, 2017) and airborne samples taken during the Comprehensive Observation Network for TRace gases by AIrLiner (CONTRAIL) project (Umezawa et al., 2012) verify the North-South gradient (shown in the supplement Sects. 2.1 and 2.2). The values of the signature of ^{13}C in CH_4 ($\delta^{13}C(CH_4)$), for example, are within the uncertainty of the CONTRAIL observations. The the signature of D in CH_4 ($\delta D(CH_4)$) is isotopological depleted in D compared to the CONTRAIL observations, however, still capture the gradient well. The vertical gradient (i.e. isotopical enrichment in the stratosphere) can be verified by comparing with balloon borne observations by Röckmann et al. (2011). Our simulation results are thereby within the local and temporal uncertainties (shown in the supplement Sect. 2.3). Note that an optimization with respect to source signatures are yet to be made and requires an optimized emission inventory. However, the capturing of the respective gradients indicates that the isotopical fractionation is sufficiently implemented.

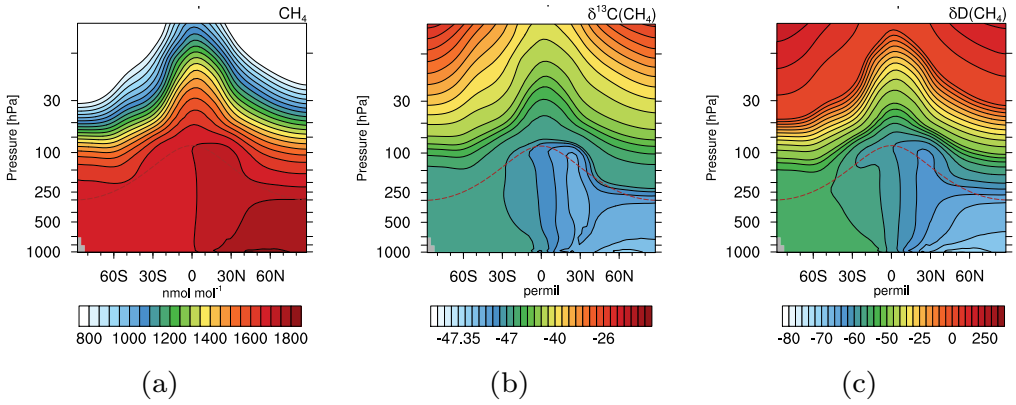

Figure 5. Zonal mean climatologies of 2000–2009 for CH_4 in [nmol mol^{-1}] (a), $\delta^{13}C(CH_4)$ in [‰] (b), and $\delta D(CH_4)$ in [‰] (c) of the simulation with EMAC and the CH4 submodel. The dashed brown lines indicate the height of the climatological tropopause.

5.3 Coupling of the CH_4 isotopologues to the isotopological hydrological cycle

The previously shown results were achieved with the CH4 submodel including the option to simulate CH_4 isotopologues. The produced HDO (by oxidation of CH_3D) is connected via the TRSYNC submodel to the isotopological hydrological cycle represented by the H2OISO submodel. We carried out an additional simulation in which we applied MECCA and MECCA_TAG to simulate the atmospheric chemistry and the CH_4 isotopologues instead of the CH4 submodel. In this simulation TRSYNC connects the produced HDO likewise to the isotopological water tracers of H2OISO.

In Figure 6 we compare the results obtained with submodel CH4 (left) and those obtained with the submodel MECCA_TAG (right) to vertical profiles of H_2O and HDO (middle) provided by the Michelson Interferometer for Passive Atmospheric Sounding (MIPAS) instrument mounted on the ENVIronmental SATellite (ENVISAT) satellite (Steinwagner et al., 2007; Lossow et al., 2011). The ENVISAT satellite is on a sun-synchronous orbit around the Earth, completing the circuit 14 times a day. The presented observational and simulated data comprise the time period July 2002 to March 2004. The vertical range of the observations extends from 6 to 68 km (i.e. approx. the range 100–1 hPa) with a vertical resolution of 3–8 km. Simulation and observation data is monthly and zonally averaged over the tropics. Similar to the conclusions of Eichinger et al. (2015a) it is observed that the EMAC model underestimates the H_2O mixing ratio (see Figs. 6a and 6c). This is associated with a too cold tropopause in EMAC, where a temperature bias of -2 to -6 K is detected in the upper troposphere, as long as the mean temperature is excluded from the nudging procedure defining the specified dynamics setup (Jöckel et al., 2016). This reduces the H_2O transported into the stratosphere since more gas phase H_2O freezes and sediments. Comparing Fig. 6d with 6f indicates a better agreement concerning the signature of D in H_2O ($\delta D(H_2O)$) in the simulation using the submodel MECCA_TAG with the MIPAS observations, which suggests that although the absolute H_2O and HDO mixing ratios are not met, the relative composition is well represented. The differences in HDO in the simulation with the CH4 submodel compared to the one with the MECCA_TAG submodel and MIPAS are potentially caused by (1) the Eq. (9) from Eichinger et al. (2015a) used in the

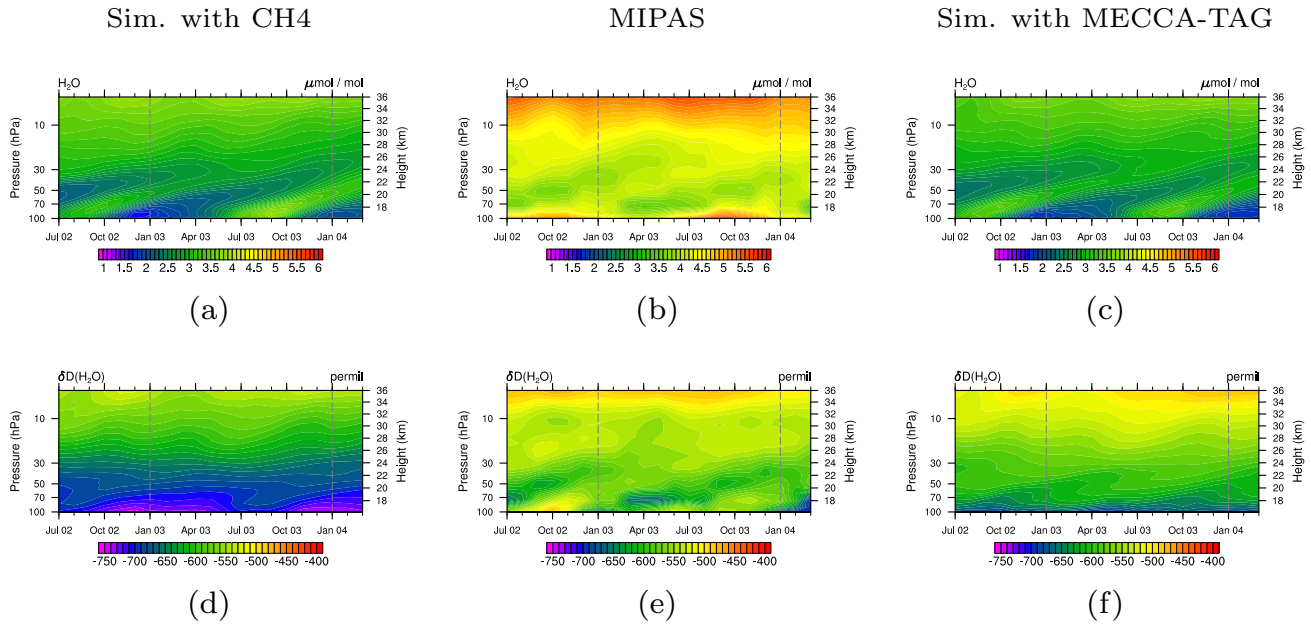

Figure 6. Tropical stratospheric tape recorder signal of H_2O (upper) and in $\delta D(H_2O)$ (lower) in MIPAS data (middle column) and the simulations with the CH4 submodel (left column) and with the MECCA_TAG submodel (right column) in the time period July 2002 to March 2004. Simulation data is averaged monthly, zonally and over the tropics between 23° S–23° N and are displayed between 100 and 1 hPa. The grey dashed lines are included for eye guidance in the comparison of the tape recorder signal.

simulation using the CH4 submodel, which possibly does not capture important fractionation processes in the oxidation chain of CH_3D, and (2) the HD, produced in the troposphere and propagating into the stratosphere, which is not included in the simplified chemistry, but represents an additional source of HDO. For an accurate simulation of stratospheric HDO this source needs to be considered as well in future simulations.

6 Summary

The submodel CH4 provides a reduced chemical set-up focusing on the CH_4 sink reactions, using predefined data of reaction partners, and optionally includes the feedback on SWV. This reduces the computational demands for sensitivity simulations of climate projections without neglecting the main source of chemically induced SWV.

We present two additional options of the CH4 submodel. The age and emission classes allow the inverse optimization of emission inventories using a fixed-lag Kalman filter. The simulation of CH_4 isotopologues provides further insight into the variability and distribution of CH_4 from its source (via emission signatures and fractionation effects) to its sink (coupling to the isotopic content of H_2O). The latter is implemented in form of the new submodel TRSYNC, which takes care of the correct and time integration conform synchronization of the various H_2O isotopologue tracers in the model.

Example use cases show specific applications of the CH4 submodel as well as the coupling to the isotopological hydrological cycle via the TRSYNC submodel, which is especially helpful for the closure of the isotopic content in SWV.

Code and data availability. The Modular Earth Submodel System (MESSy) is continuously further developed and applied by a consortium of institutions. The usage of MESSy and access to the source code is licensed to all affiliates of institutions which are members of the MESSy Consortium. Institutions can become a member of the MESSy Consortium by signing the MESSy Memorandum of Understanding. More information can be found on the MESSy Consortium Web-site (http://www.messy-interface.org). The new submodels presented in this paper have been implemented based on MESSy v2.53.0 and are available since v2.54.0. The exact code version used to produce the examples is archived at the German Climate Computing Center (DKRZ) and can be made available to members of the MESSy community upon request.

Author contributions. FW and PJ worked on the development of the CH4 and TRSYNC submodel and wrote the manuscript.

Competing interests. The authors declare that they have no conflict of interest.

Acknowledgements. We acknowledge the DLR internal project KliSAW (Klimarelevanz von atmosphärischen Spurengasen, Aerosolen und Wolken), which provided the financial basis for the presented model developments, and the Helmholtz-Gemeinschaft e.V. (HGF) "Project Advanced Earth System Modelling Capacity (ESM)". The model simulations have been performed at the German Climate Computing Centre (DKRZ) through support from the Bundesministerium für Bildung und Forschung (BMBF). We further thank Theresa Klausner and two anonymous reviewers for their supportive comments on the manuscript.

References

Austin, J., Wilson, J., Li, F., and Vömel, H.: Evolution of Water Vapor Concentrations and Stratospheric Age of Air in Coupled Chemistry-Climate Model Simulations, Am. Met. Soc., pp. 905–921, https://doi.org/10.1175/JAS3866.1, 2007.

Bergamaschi, P., Brühl, C., Brenninkmeijer, C. A. M., Saueressig, G., Crowley, J. N., Grooß, J. U., Fischer, H., and Crutzen, P. J.: Implications of the large carbon kinetic isotope effect in the reaction CH_4 + Cl for the $^{13}C/^{12}C$ ratio of stratospheric CH_4, Geophys. Res. Lett., 23, 2227–2230, https://doi.org/10.1029/96GL02139, 1996.

Bigeleisen, J.: Isotope Effects in Chemistry and Biology, chap. Chapter 01 Theoretical Basis of Isotope Effects from an Autobiographical Perspective, pp. 1–40, Taylor & Taylor & Francis Group, LLC, https://doi.org/10.1201/9781420028027.ch1, http://dx.doi.org/10.1201/9781420028027.ch1, 2005.

Boville, B. A., Kiehl, J. T., Rasch, P. J., and Bryan, F. O.: Improvements to the NCAR CSM-1 for Transient Climate Simulations, J. Climate, 14, 164–179, https://doi.org/10.1175/1520-0442(2001)014<0164:ITTNCF>2.0.CO;2, 2001.

Bruhwiler, L. M. P., Michalak, A. M., Peters, W., Baker, D. F., and Tans, P.: An improved Kalman Smoother for atmospheric inversions, Atmos. Chem. Phys., 5, 2691–2702, https://doi.org/10.5194/acp-5-2691-2005, https://www.atmos-chem-phys.net/5/2691/2005/, 2005.

Crowley, J. N., Saueressig, G., Bergamaschi, P., Fischer, H., and Harris, G. W.: Carbon kinetic isotope effect in the reaction CH_4+Cl: a relative rate study using FTIR spectroscopy, Chem. Phys. Lett., 303, 268–274, https://doi.org/10.1016/S0009-2614(99)00243-2, 1999.

Dee, D. P., Uppala, S. M., Simmons, A. J., Berrisford, P., Poli, P., Kobayashi, S., Andrae, U., Balmaseda, M. A., Balsamo, G., Bauer, P., Bechtold, P., Beljaars, A. C. M., van de Berg, L., Bidlot, J., Bormann, N., Delsol, C., Dragani, R., Fuentes, M., Geer, A. J., Haimberger, L., Healy, S. B., Hersbach, H., Hólm, E. V., Isaksen, L., Kållberg, P., Köhler, M., Matricardi, M., McNally, A. P., Monge-Sanz, B. M., Morcrette, J.-J., Park, B.-K., Peubey, C., de Rosnay, P., Tavolato, C., Thépaut, J.-N., and Vitart, F.: The ERA-Interim reanalysis: configuration and performance of the data assimilation system, Quart. J. Roy. Meteor. Soc., 137, 553–597, https://doi.org/10.1002/qj.828, http://dx.doi.org/10.1002/qj.828, 2011.

ECMWF: IFS DOCUMENTATION - Cy31r1, Part IV: Physical Processes, https://www.ecmwf.int/sites/default/files/elibrary/2007/9221-part-iv-physical-processes.pdf, 2007.

Eichinger, R.: Investigation of stratospheric water vapour by means of the simulation of water isotopologues, Ph.D. thesis, Ludwig Maximilian Universität München, 2014.

Eichinger, R., Jöckel, P., Brinkop, S., Werner, M., and Lossow, S.: Simulation of the isotopic composition of stratospheric water vapour - Part 1: Description and evaluation of the EMAC model, Atmos. Chem. Phys., 15, 5537–5555, https://doi.org/10.5194/acp-15-5537-2015, 2015a.

Eichinger, R., Jöckel, P., and Lossow, S.: Simulation of the isotopic composition of stratospheric water vapour - Part 2: Investigation of HDO / H_2O variations, Atmos. Chem. Phys., 15, 7003–7015, https://doi.org/10.5194/acp-15-7003-2015, http://www.atmos-chem-phys.net/15/7003/2015/, 2015b.

Fletcher, M., E., S., Tans, P. P., Bruhwiler, L. M., Miller, J. B., and Heimann, M.: CH_4 sources estimated from atmospheric observations of CH_4 and its $^{13}C/^{12}C$ isotopic ratios: 2. Inverse modeling of CH_4 fluxes from geographical regions, Glob. Biogeochem. Cycles, 18, 1–15, https://doi.org/10.1029/2004GB002224, 2004.

Frank, F.: Atmospheric methane and its isotopic composition in a changing climate: A modelling study, Ph.D. thesis, Ludwigs Maximillian Universität München, 2018.

Frank, F., Jöckel, P., Gromov, S., and Dameris, M.: Investigating the yield of H_2O and H_2 from methane oxidation in the stratosphere, Atmos. Chem. Phys., 18, 9955–9973, https://doi.org/10.5194/acp-18-9955-2018, https://www.atmos-chem-phys.net/18/9955/2018/, 2018.

Gromov, S., Jöckel, P., Sander, R., and Brenninkmeijer, C. A. M.: A kinetic chemistry tagging technique and its application to modelling the stable isotopic composition of atmospheric trace gases, Geosci. Model Dev., 3, 337–364, https://doi.org/10.5194/gmd-3-337-2010, www.geosci-model-dev.net/3/337/2010/, 2010.

Hein, R., Crutzen, P. J., and Heimann, M.: An inverse modeling approach to investigate the global atmospheric methane cycle, Glob. Biogeochem. Cycles, 11, 43–76, 1997.

Holmgren, P.: Global land use area change matrix, Working Paper 134, Forest Resources Assessment Programme, Food and Agriculture Organization of the United Nations, 2006.

IPCC: Climate Change 2013: The Physical Science Basis. Contribution of Working Group I to the Fifth Assessment Report of the Intergovernmental Panel on Climate Change, Cambridge University Press, Cambridge, United Kingdom and New York, NY, USA, https://doi.org/10.1017/CBO9781107415324, www.climatechange2013.org, 2013.

Jöckel, P., Kerkweg, A., Pozzer, A., Sander, R., Tost, H., Riede, H., Baumgaertner, A., Gromov, S., and Kern, B.: Development cycle 2 of the Modular Earth Submodel System MESSy2, Geosci. Model Dev., 3, 717–752, https://doi.org/10.5194/gmd-3-717-2010, manual, 2010.

Jöckel, P., Tost, H., Pozzer, A., Kunze, M., Kirner, O., Brenninkmeijer, C. A. M., Brinkop, S., Cai, D. S., Dyroff, C., Eckstein, J., Frank, F., Garny, H., Gottschaldt, K.-D., Graf, P., Grewe, V., , Kerkweg, A., Kern, B., Matthes, S., Mertens, M., Meul, S., Neumaier, M., Nützel, M., Oberländer-Hayn, S., Ruhnke, R., Runde, T., Sander, R., Scharffe, D., and Zahn, A.: Earth System Chemistry integrated Modelling (ESCiMo) with the Modular Earth Submodel System (MESSy) version 2.51, Geosci. Model Dev., 9, 1153–1200, https://doi.org/10.5194/gmd-9-1153-2016, http://www.geosci-model-dev.net/9/1153/2016/gmd-9-1153-2016.html, 2016.

Kerkweg, A., Buchholz, J., Ganzeveld, L., Pozzer, A., Tost, H., and Jöckel, P.: Technical Note: An implementation of the dry removal processes DRY DEPosition and SEDImentation in the Modular Earth Submodel System (MESSy), Atmos. Chem. Phys., 6, 4617–4632, https://doi.org/10.5194/acp-6-4617-2006, https://www.atmos-chem-phys.net/6/4617/2006/, 2006a.

Kerkweg, A., Sander, R., Tost, H., and Jöckel, P.: Technical note: Implementation of prescribed (OFFLEM), calculated (ONLEM), and pseudo-emissions (TNUDGE) of chemical species in the Modular Earth Submodel System (MESSy), Atmos. Chem. Phys., 6, 3603–3609, https://doi.org/10.5194/acp-6-3603-2006, https://www.atmos-chem-phys.net/6/3603/2006/, 2006b.

King, G.: Responses of atmospheric methane consumption by soils to global climate change, Global Change Biology, 3, 351–362, https://doi.org/10.1046/j.1365-2486.1997.00090.x, http://dx.doi.org/10.1046/j.1365-2486.1997.00090.x, 1997.

Kirschke, S., Bousquet, P., Ciais, P., Saunois, M., Canadell, J. G., Dlugokencky, E. J., Bergamaschi, P., Bergmann, D., Blake, D. R., Bruhwiler, L., Cameron-Smith, P., Castaldi, S., Chevallier, F., Feng, L., Fraser, A., Heimann, M., Hodson, E. L., Houweling, S., Josse, B., Fraser, P. J., Krummel, P. B., Lamarque, J.-F., Langenfelds, R. L., Le Quèrè, C., Naik, V., O'Doherty, S., Palmer, P. I., Pison, I., Plummer, D., Poulter, B., Prinn, R. G., Rigby, M., Ringeval, B., Santini, M., Schmidt, M., Shindell, D. T., Simpson, I. J., Spahni, R., Steele, L. P., Strode, S. A., Sudo, K., Szopa, S., van der Werf, G. R., Voulgarakis, A., van Weele, M., Weiss, R. F., Williams, J. E., and Zeng, G.: Three decades of global methane sources and sinks, Nature Geoscience, 6, 813–823, https://doi.org/10.1038/ngeo1955, https://www.nature.com/articles/ngeo1955#supplementary-information, 2013.

le Texier, H., Solomon, S., and Garcia, R. R.: The role of molecular hydrogen and methane oxidation in the water vapour budget of the stratosphere, Quart. J. Roy. Meteor. Soc., 114, 281–295, https://doi.org/10.1002/qj.49711448002, 1988.

Lossow, S., Steinwagner, J., Urban, J., Dupuy, E., Boone, C. D., Kellmann, S., Linden, A., Kiefer, M., Grabowski, U., Glatthor, N., Höpfner, M., Röckmann, T., Murtagh, D. P., Walker, K. A., Bernath, P. F., von Clarmann, T., and Stiller, G. P.: Comparison of

HDO measurements from Envisat/MIPAS with observations by Odin/SMR and SCISAT/ACE-FTS, Atmos. Meas. Tech., 4, 1855–1874, https://doi.org/10.5194/amt-4-1855-2011, https://www.atmos-meas-tech.net/4/1855/2011/, 2011.

Maxfield, P. J., Evershed, R. P., and Hornibrook, E. R. C.: Physical and Biological Controls on the In Situ Kinetic Isotope Effect Associated with Oxidation of Atmospheric CH_4 in Mineral Soils, Environ. Sci. Technol., 42, 7824–7830, https://doi.org/10.1021/es800544q, http://dx.doi.org/10.1021/es800544q, pMID: 19031867, 2008.

Monge-Sanz, B. M., Chipperfield, M. P., Untch, A., Morcrette, J.-J., Rap, A., and Simmons, A. J.: On the uses of a new linear scheme for stratospheric methane in global models: water source, transport tracer and radiative forcing, Atmos. Chem. Phys., 13, 9641–9660, https://doi.org/10.5194/acp-13-9641-2013, https://www.atmos-chem-phys.net/13/9641/2013/, 2013.

Monteil, G., Houweling, S., Dlugockenky, E. J., Maenhout, G., Vaughn, B. H., White, J. W. C., and Rockmann, T.: Interpreting methane variations in the past two decades using measurements of CH_4 mixing ratio and isotopic composition, Atmos. Chem. Phys., 11, 9141–9153, 2011.

Mote, P.: The annual cycle of stratospheric water vapor in a general circulation model, J. Geophys. Res., 100, 7363–7379, https://doi.org/10.1029/94JD03301, http://onlinelibrary.wiley.com/doi/10.1029/94JD03301/pdf, 1995.

Nair, H., Summers, M. E., Miller, C. E., and Yung, Y. L.: Isotopic fractionation of methane in the martian atmosphere, ICARUS, 175, 32–35, https://doi.org/10.1016/j.icarus.2004.10.018, 2005.

Nickl, A.-L., Mertens, M., Roiger, A., Fix, A., Amediek, A., Fiehn, A., Gerbig, C., Galkowski, M., Kerkweg, A., Klausner, T., Eckl, M., and Jöckel, P.: Forecasting of regional methane from coal mine emissions in the Upper Silesian Coal Basin using the on-line nested global regional chemistry climate model MECO(n)(MESSy v2.53), Geosci. Model Dev. Discuss., 2019, 1–29, https://doi.org/10.5194/gmd-2019-303, https://www.geosci-model-dev-discuss.net/gmd-2019-303/, 2019.

Nisbet, E. G., Dlugokencky, E. J., Manning, M. R., Lowry, D., Fisher, R. E., France, J. L., Michel, S. E., Miller, J. B., White, J. W. C., Vaughn, B., Bousquet, P., Pyle, J. A., Warwick, N. J., Cain, M., Brownlow, R., Zazzeri, G., Lanoisellé, M., Manning, A. C., Gloor, E., Worthy, D. E. J., Brunke, E.-G., Labuschangne, C., W., W. E., and Ganesan, A. L.: Rising atmospheric methane: 2007–2014 growth and isotopic shift, Glob. Biogeochem. Cycles, 30, 1–15, https://doi.org/10.1002/2015GB005326.Received, 2016.

Nixon, C. A., Temelso, B., Vinatier, S., Teanby, N. A., B'ezard, B., Achterberg, R. K., Mandt, K. E., Sherrill, C. D., Irwin, P. G. J., Jennings, D. E., Romani, P. N., Coustenis, A., and Flasar, F. M.: Isotopic ratios in titan's methane: measurements and modeling, The Astrophysical Journal, 749, 159, https://doi.org/10.1088/0004-637X/749/2/159, http://stacks.iop.org/0004-637X/749/i=2/a=159, 2012.

Olivier, J. and Janssens-Maenhout, G.: CO2 Emissions from Fuel Combustion 2012, chap. Part III, Greenhouse-Gas Emissions, p. 540, International Energy Agency, https://doi.org/https://doi.org/https://doi.org/10.1787/co2_fuel-2012-en, https://www.oecd-ilibrary.org/content/publication/co2_fuel-2012-en, 2012.

Revell, L. E., Bodeker, G. E., Huck, P. E., Williamson, B. E., , and Rozanov, E.: The sensitivity of stratospheric ozone changes through the 21st century to N_2O and CH_4, Atmos. Chem. Phys., 12, 11 309–11 317, https://doi.org/10.5194/acp-12-11309-2012, www.atmos-chem-phys.net/12/11309/2012/, 2012.

Rigby, M., Manning, A. J., and Prinn, R. G.: The value of high-frequency high-precision methane isotopologue measurements for source and sink estimation, J. Geophys. Res., 117, D12 312, https://doi.org/10.1029/2011JD017384, 2012.

Röckmann, T., Brass, M., Borchers, R., and Engel, A.: The isotopic composition of methane in the stratosphere: high-altitude balloon sample measurements, Atmos. Chem. Phys., 11, 13 287–13 304, https://doi.org/10.5194/acp-11-13287-2011, 2011.

Roeckner, E., Brokopf, R., Esch, M., Giorgetta, M., Hagemann, S., Kornblueh, L., Manzini, E., Schlese, U., and Schulzweida, U.: Sensitivity of Simulated Climate to Horizontal and Vertical Resolution in the ECHAM5 Atmosphere Model, American Meterological Society, 19, 3771–3791, 2006.

Sander, R., Kerkweg, A., Jöckel, P., and Lelieveld, J.: Technical note: The new comprehensive atmospheric chemistry module MECCA, Atmos. Chem. Phys., 5, 445–450, 2005.

Sander, R., Jöckel, P., Kirner, O., Kunert, A. T., Landgraf, J., and Pozzer, A.: The photolysis module JVAL-14, compatible with the MESSy standard, and the JVal PreProcessor (JVPP), Geosci. Model Dev., 7, 2653–2662, https://doi.org/10.5194/gmd-7-2653-2014, www.geosci-model-dev.net/7/2653/2014/, 2014.

Sander, S. P., Abbatt, J., Barker, J. R., Burkholder, J. B., Friedl, R. R., Golden, D. M., Huie, R. E., Kolb, C. E., Kurylo, M. J., Moortgat, G. K., Orkin, V. L., and Wine, P. H.: Chemical Kinetics and Photochemical Data for Use in Atmospheric Studies, Evaluation No. 17, JPL Publication 10-6, Jet Propulsion Laboratory, https://doi.org/10.1002/kin.550171010, http://jpldataeval.jpl.nasa.gov/, 2011.

Saueressig, G., Bergamaschi, P., Crowley, J. N., and Fischer, H.: Carbon kinetic isotope effect in the reaction of CH_4 with Cl atoms, Geophys. Res. Lett., 22, 1225–1228, 1995.

Saueressig, G., Bergamaschi, P., Crowley, J., and Fischer, H.: D/H kinetic isotope effect in the reaction CH_4 + Cl, Geophys. Res. Lett., 23, 3619–3622, 1996.

Saueressig, G., Crowley, J. N., Bergamaschi, P., Brühl, C., Brenninkmeijer, C. A. M., and Fischer, H.: Carbon 13 and D kinetic isotope effects in the reactions of CH_4 with $O^1(D)$ and OH: New laboratory measurements and their implications for the isotopic composition of stratospheric methane, J. Geophys. Res., 106, 23 127–23 138, 2001.

Saunois, M., Bousquet, P., Poulter, B., Peregon, A., Ciais, P., Canadell, J. G., Dlugokencky, E. J., Etiope, G., Bastviken, D., Houweling, S., Janssens-Maenhout, G., Tubiello, F. N., Castaldi, S., Jackson, R. B., Alexe, M., Arora, V. K., Beerling, D. J., Bergamaschi, P., Blake, D. R., Brailsford, G., Brovkin, V., Bruhwiler, L., Crevoisier, C., Crill, P., Covey, K., Curry, C., Frankenberg, C., Gedney, N., Höglund-Isaksson, L., Ishizawa, M., Ito, A., Joos, F., Kim, H.-S., Kleinen, T., Krummel, P., Lamarque, J.-F., Langenfelds, R., Locatelli, R., Machida, T., Maksyutov, S., McDonald, K. C., Marshall, J., Melton, J. R., Morino, I., Naik, V., O'Doherty, S., Parmentier, F.-J. W., Patra, P. K., Peng, C., Peng, S., Peters, G. P., Pison, I., Prigent, C., Prinn, R., Ramonet, M., Riley, W. J., Saito, M., Santini, M., Schroeder, R., Simpson, I. J., Spahni, R., Steele, P., Takizawa, A., Thornton, B. F., Tian, H., Tohjima, Y., Viovy, N., Voulgarakis, A., van Weele, M., van der Werf, G. R., Weiss, R., Wiedinmyer, C., Wilton, D. J., Wiltshire, A., Worthy, D., Wunch, D., Xu, X., Yoshida, Y., Zhang, B., Zhang, Z., and Zhu, Q.: The global methane budget 2000–2012, Earth Syst. Sci. Data, 8, 697–751, https://doi.org/10.5194/essd-8-697-2016, https://www.earth-syst-sci-data.net/8/697/2016/, 2016.

Schaefer, H., Fletcher, S. E. M., Veidt, C., Lassey, K. R., Brailsford, G. W., Bromley, T. M., Dlugokencky, E. J., Michel, S. E., Miller, J. B., Levin, I., Lowe, D. C., Martin, R. J., Vaughn, B. H., and White, J. W. C.: A 21st century shift from fossil-fuel to biogenic methane emissions indicated by $^{13}CH_4$, Science (New York, N.Y.), 352, 80–84, https://doi.org/10.1126/science.aad2705, http://science.sciencemag.org/content/352/6281/80.abstract, 2016.

Snover, A. and Quay, P.: Hydrogen and carbon kinetic isotope effects during soil uptake of atmospheric methane and a temperate grassland, Glob. Biogeochem. Cycles, 14, 25–39, 2000.

Solomon, S., Rosenlof, K. H., Portmann, R. W., Daniel, J. S., Davis, S. M., Sanford, T. J., and Plattner, G.-K.: Contributions of Stratospheric Water Vapor to Decadal Changes in the Rate of Global Warming, Science, 327, 1219–1223, https://doi.org/10.1126/science.1182488, 2010.

Steinwagner, J., Milz, M., von Clarmann, T., Glatthor, N., Grabowski, U., Höpfner, M., Stiller, G. P., and Röckmann, T.: HDO measurements with MIPAS, Atmos. Chem. Phys., 7, 2601–2615, https://doi.org/10.5194/acp-7-2601-2007, https://www.atmos-chem-phys.net/7/2601/2007/, 2007.

Stenke, A. and Grewe, V.: Simulation of stratospheric water vapor trends: impact on stratospheric ozone chemistry, Atmos. Chem. Phys., 5, 1257–1272, www.atmos-chem-phys.org/acp/5/1257/, 2005.

Stolper, D., Sessions, A., Ferreira, A., Neto, E. S., Schimmelmann, A., Shusta, S., Valentine, D., and Eiler, J.: Combined C–D and D–D clumping in methane: Methods and preliminary results, Geochim. Cosmochim. Acta, 126, 169–191, https://doi.org/10.1016/j.gca.2013.10.045., http://www.sciencedirect.com/science/article/pii/S0016703713006170, 2014.

Tian, W., Chipperfield, M. P., and Lü, D.: Impact of increasing stratospheric water vapor on ozone depletion and temperature change, Advances in Atmospheric Sciences, 26, 423–437, https://doi.org/10.1007/s00376-009-0423-3, https://doi.org/10.1007/s00376-009-0423-3, 2009.

Tost, H., Jöckel, P., Kerkweg, A., Sander, R., and Lelieveld, J.: Technical note: A new comprehensive SCAVenging submodel for global atmospheric chemistry modelling, Atmos. Chem. Phys., 6, 565–574, https://doi.org/10.5194/acp-6-565-2006, https://www.atmos-chem-phys.net/6/565/2006/, 2006.

Umezawa, T., MacHida, T., Ishijima, K., Matsueda, H., Sawa, Y., Patra, P. K., Aoki, S., and Nakazawa, T.: Carbon and hydrogen isotopic ratios of atmospheric methane in the upper troposphere over the Western Pacific, Atmos. Chem. Phys., 12, 8095–81 113, https://doi.org/10.5194/acp-12-8095-2012, 2012.

White, J., Vaughn, B., and Michel, S.: University of Colorado, Institute of Arctic and Alpine Research (INSTAAR), Stable Isotopic Composition of Atmospheric Methane (^{2}H) from the NOAA ESRL Carbon Cycle Cooperative Global Air Sampling Network, 2005-2009, Version: 2016-04-26, ftp://aftp.cmdl.noaa.gov/data/trace_gases/ch4h2/flask/, 2016.

White, J., Vaughn, B., and Michel, S.: University of Colorado, Institute of Arctic and Alpine Research (INSTAAR), Stable Isotopic Composition of Atmospheric Methane (^{13}C) from the NOAA ESRL Carbon Cycle Cooperative Global Air Sampling Network, 1998-2016, Version: 2018-01-31, ftp://aftp.cmdl.noaa.gov/data/trace_gases/ch4c13/flask/, 2017.

Winterstein, F., Tanalski, F., Jöckel, P., Dameris, M., and Ponater, M.: Implication of strongly increased atmospheric methane concentrations for chemistry–climate connections, Atmos. Chem. Phys., 19, 7151–7163, https://doi.org/10.5194/acp-19-7151-2019, https://www.atmos-chem-phys.net/19/7151/2019/, 2019.